Double capture into autoionizing states in low-energy He^{2+}-, Li^{3+}-, and B^{5+}-H_2 collisions

Ingjald Pilskog,[1,2] Nicolas Sisourat,[1,3] Jérémie Caillat,[1,3] and Alain Dubois[1,3]

[1]*Laboratoire de Chimie Physique - Matière et Rayonnement, UMR 7614, UPMC Université Paris 6, 11 rue Pierre et Marie Curie, F-75231 Paris Cedex 05, France*

[2]*Department of Physics and Technology, University of Bergen, N-5007 Bergen, Norway*

[3]*LCPMR, UMR 7614, CNRS, F-75005 Paris, France*

(Received 30 December 2011; revised manuscript received 14 March 2012; published 12 April 2012)

A theoretical investigation of double capture into autoionizing states are presented for collisions between fully stripped low-charge ions and dihydrogen molecules at impact energies ranging from 0.05 to 25 keV/u. The state-to-state cross sections stem from a nonperturbative semiclassical treatment, using asymptotic states expansions with proper translational conditions and taking into account statically and dynamically interelectronic correlation in a configuration interaction approach. The results are presented for three projectiles (He^{2+}, Li^{3+}, and B^{5+}) and discussed in the context of future interferometric collision experimental investigations as well as further improvements in the coherent description of the decay of the autoionizing states populated in the scattering stage.

DOI: 10.1103/PhysRevA.85.042712 PACS number(s): 34.70.+e

I. INTRODUCTION

The study of (valence- or inner-shell) highly excited, including multiply excited, atomic or molecular species is of great importance to understand the response of matter under strong external perturbations which can be created by either electromagnetic fields [1–3] or charged particle beams (electron [4,5] or ion [6–8]). In this context experimental and theoretical coupled studies are very challenging since, in order to be complete and probe quantum mechanics at its most fundamental level, they must involve sophisticated detection and multicoincidence techniques (the so-called "perfect scattering experiments," cf. [9]) as well as a thorough knowledge of these exotic structures and of their dynamics during and after the scattering event. The measurements or predictions of the cross sections for the production of highly excited atomic or molecular structures are also important from a practical point of view [10,11].

In the case of heavy charged particle impact—which will only be considered in the following—a wealth of data have been produced to understand the mechanisms responsible for the outcome of the scattering event. From a fundamental point of view, multiply excited atomic or molecular species created by ion impact are stimulating quantum objects to study the static and dynamical effects of electron-electron interaction imbedded in the strong time-dependent Coulombic interactions between the projectile and target nuclei (or cores) and the various active electrons (cf., for example, the review of Belkić *et al.* [12] for high energy collisions). Collisions involving asymmetric systems, such as multiply charged ions and closed shell atoms (e.g., rare gases) or simple molecules (H_2, CO, CO_2, ...), have therefore attracted a lot of attention in the last two to three decades (for example, among many others, [6,13–22]). The large difference in the first ionization threshold of the two scattering partners allows the production of (specific) multiply excited species which are in general autoionizing. However even for pure two-electron systems (e.g., a fully stripped projectile with He or H_2), it is not possible to state that the processes are well understood and routinely modeled [23,24]. Indeed in the low and intermediate impact energy ranges considered in the following, the various stages to consider in the theoretical description of these systems are (i) to treat nonperturbatively the scattering event (see, for example, [25,26] and more specifically for atomic targets [27–32] and for molecular ones [23,33,34]), (ii) to accurately describe the multiply excited states (e.g., [35–40]) and to involve them in the close-coupling scheme, (iii) to include, if relevant, the possible decay of these autoionizing states during the scattering stage (e.g. [41–43]), i.e., in the presence of the outgoing projectile, and finally (iv) to model the further scattering of the ejected electrons onto the fragments created by the two—successive or quasisimultaneous—processes; see [7,44] in the context of the study of interference effects. Although the various stages have been investigated separately, there is no theoretical coherent description of such complex multistep dynamics; cf. the conclusive remarks in Salin's review [45].

The present study follows this guideline and is focused on the first two stages of the description of double capture into autoionizing states (ADC) in slow collisions between fully stripped low-charge ions and a H_2 molecule. The original driving force of our work is the interferometric scattering experiments proposed by Barrachina and Zitnik [44] and performed by Chesnel *et al.* [7] (see also [46,47]), whose extension to low impact energies would be able to probe with ultimate details the four stages described above. However since the ADC cross sections for the collision system chosen originally by the experimentalists (He^{2+}-H_2) were proved to decrease drastically for energies below 8 keV [46], the first stage of our investigation is to select a more convenient projectile. In this paper we therefore consider the two projectiles Li^{3+} and B^{5+}, in comparison with the He^{2+} case, at energies ranging from 0.05 to 25 keV/u and analyze the ADC process in detail, i.e., at the level of all important autoionizing states populated during the scattering. The cross sections have been obtained by the use of a semiclassical coupled-channel approach based on asymptotic channels expansion (ACCC) which has recently been developed [48], and would serve as benchmarks for future experimental and independent theoretical investigations.

The manuscript is organized as follows. Section II is devoted to a short description of the ACCC approach and of the methods we used to identify and select the numerous

autoionizing states included in the computations. In Sec. III we present the results of our calculations: the total ADC cross sections as functions of impact energy and the state-to-state cross sections for two typical velocities are presented in graphical as well as tabular forms and discussed. The manuscript ends with an Appendix where we show for comparison some results obtained from smaller basis sets.

Atomic units are used in the following, unless otherwise stated.

II. METHODS

A. The ACCC approach and cross sections

We have presented in a recent paper [48] the original approach that we developed for the description of the two-electron processes occurring during ion-molecule or ion-atom collisions. We therefore give only a brief description of the theory in the following.

In this approach the collision is treated by the well established straight-line impact parameter method [26] where the projectile-target relative motion is treated classically and the electronic degrees of freedom are treated quantally in a nonperturbative scheme with a Hamiltonian containing all electrostatic potentials between the five involved charged particles. However the nuclei of the molecular target are frozen in space (rovibrational sudden approximation) preventing us from exploring too low energies, below about 10 eV/u [48]. The time-dependent Schrödinger equation (TDSE) of the two-electron system is solved by expanding the scattering wave function onto a basis set composed of states describing the two collision partners at infinite separation, i.e.: (i) two-electron molecular states on the target (describing the initial state and excitation channels, plus ionization through pseudostates), (ii) two-electron atomic states on the projectile (for double capture channels), and (iii) the products of one-electron states centered on the target and the projectile (to describe, for example, simple transfer or transfer-excitation). These states are augmented by plane-wave electron translational factors (PW-ETF) to take into account the relative motion of the two collision partners and ensure Galilean invariance of the results. These three different components are antisymmetrized and only singlet terms are included in the calculations due to spin conservation with the initial state of the collision (ground state of H_2, $X^1\Sigma_g^+$). These states are expressed in terms of Gaussian-type orbitals (GTO) whose exponents have been optimized to match the spectroscopic data of the considered species. All couplings terms, including the interelectronic repulsion, between these states are evaluated on a temporal grid corresponding to important relative positions between the target and the projectile: this stage is extremely demanding in the computations since it involves the evaluation of multiple integrals, the most complex ones being the three-center two-electron matrix elements with PW-ETFs. The set of coupled differential equations equivalent to the TDSE within the basis set representation is then solved. After sufficiently long propagation time the probability amplitudes related to the different states included in the basis set allow us to evaluate the cross sections of the processes under consideration. We should finally stress that this evaluation should be performed for different molecular orientations with respect to the projectile beam and internuclear distances; to keep the calculations within a reasonable CPU time, we performed the averaging procedure for the molecular orientation using three perpendicular geometries and the target was fixed to its equilibrium internuclear distance ($R_{eq} = 1.4$ a.u. for H_2); cf. Eqs. (11) and (12) in [48].

B. Basis set and autoionizing states

In atomic or molecular species the autoionizing (AI) states are imbedded in the continuum as resonant states. However we formulate their description within a discrete basis expressed in terms of GTOs which give well described bound states (i.e., ground and singly excited states) while the continuum is represented by pseudostates which are intermixed with the AI states. This makes the task of their selection, identification, and optimization very awkward. In the present paper [49] we have developed Li^{2+} and Li^+ basis sets onto 36 (12 $\ell = 0$ and 3×8 $\ell = 1$) GTOs and 666 spin-adapted products of GTOs so that 167 two-electron states were kept after diagonalization, many of them being pseudostates. For B^{4+} and B^{3+} the basis set is composed of 35 GTOs (14 $\ell = 0$ and 3×7 $\ell = 1$) and 630 GTO products for a total of 185 two-electron states. The cross sections presented in the following have been obtained using these basis sets and their convergence has been checked with smaller ones: we present and comment in the Appendix on the cross sections computed with restricted basis sets for two typical velocities.

In our previous paper [48], the autoionizing states were identified using the virial theorem. This is a necessary, but not sufficient, criterion for identifying resonant states. Indeed for Li^{3+} and B^{5+} projectiles the GTO basis sets are so large that the number of resonant states and pseudostates included in our calculations increases the probability for pseudostates to lie sufficiently close to a resonant state such that the virial theorem may wrongly categorized them as resonant states. This happens to such a degree that the method cannot be considered viable and adds up to the difficulty of identification of the B^{3+} high lying AI states for which little is known in the literature. In order to further investigate these states in the present work, we have therefore used the so-called stabilization (or scaling) method; cf. [50–53] and references therein. In short this method involves the diagonalization of the two-electron atom (or ion) Hamiltonian in a position space scaled by some parameter η, i.e., the electronic position vectors $\vec{r}_i$ are transformed into $\vec{\rho}_i = \eta\vec{r}_i$. Since bound and resonant states are confined around the nucleus, they are well described with a given Gaussian basis set centered on the nucleus, even upon (reasonable) scaling. On the contrary, pseudostates, modeling continuum states, are delocalized and therefore their description with the given set of Gaussian exponents will change drastically with the scaling parameter. The states obtained by this procedure present thus two kinds of behavior when varying η: the values of the resonant state energies present a near independence upon the scaling parameter while the energies of the pseudostates vary dramatically with η. As an example Fig. 1 shows a selection of the He energy levels (black dots) obtained by diagonalization with the basis set described above, as a function of the parameter η. The spectrum shows

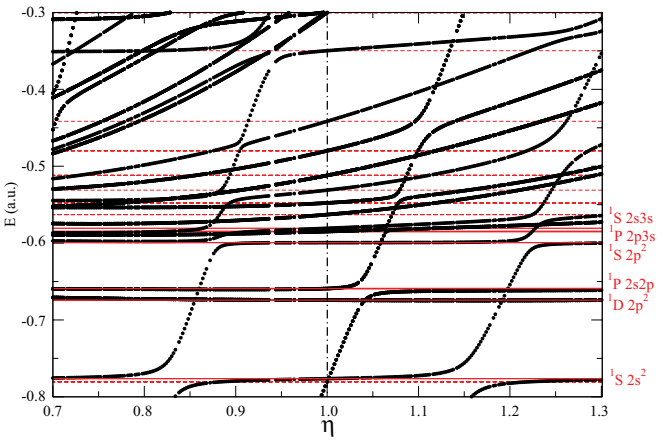

FIG. 1. (Color online) Spectrum of He in a selected range of energy where low lying AI singlet states are observed, as functions of the scaling parameter η. The calculations are shown in black dots. The red solid lines show the actual values of some of the doubly excited states, identified on the right side by their terms and corresponding electronic configurations. The red dashed lines show the energies of the pseudostates included in the present basis set.

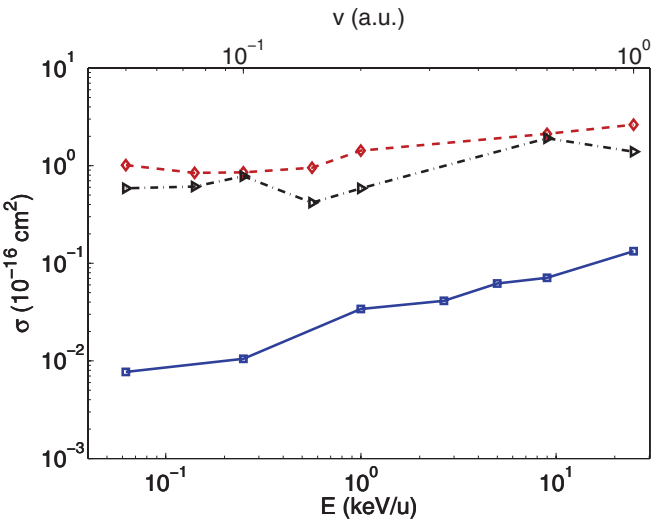

FIG. 2. (Color online) Total ADC cross sections are shown as functions of impact energy (bottom axis) and velocity (top axis) for three projectiles: He^{2+} blue solid line, Li^{3+} red dashed line, and B^{5+} black dotted-dashed line.

a series of stable states whose energies converge to the exact values (red solid lines) obtained for $\eta = 1$ (no scaling). One can observe in this spectrum that the pseudostates which diverge with increasing η cause avoided crossings (due to symmetry reasons) with the series of stable states. The red dashed lines show the energies of some of the pseudostates kept in the basis set.

Note finally that the energies and terms of the important doubly excited electronic configurations included in our calculations are shown in Tables I, II, and III for He, Li^+, and B^{3+}, respectively.

III. RESULTS AND DISCUSSION

The results for Li^{3+}-H_2 and B^{5+}-H_2 presented in the following have been obtained with the basis sets described above. To ensure the convergence of the results, the two parameters to define the trajectory were fixed as following: the relative projectile-target distance which defines the start and the end of the propagation was fixed to 40 a.u. for both projectiles. Within this range the coupling and overlap matrix elements have been evaluated at 400 equally spaced projectile-target relative positions. The results for He^{2+}-H_2 are equivalent to the ones presented in our recent work [48] but in the present paper the state-to-state cross sections are also analyzed.

In Fig. 2 the cross sections of total double capture to doubly excited states are presented as functions of impact energy and velocity for the three systems under consideration. Striking differences distinguish Li^{3+} and B^{5+} from He^{2+}: (i) for the first two projectiles the cross sections are close to each other and larger by one to two orders of magnitude compared to He^{2+}, and (ii) the amplitude of variations of the cross sections is about 4, showing a slight oscillatory behavior, while for the latter case they decrease by a factor of 20 with decreasing energies. This strong difference in the magnitude of the cross sections is mainly due to an energetic effect. Indeed the doubly excited He states lie much above the initial channel (in fact at least 30 eV above the H_2 ground state, named X in the following; cf. Table I): considering a molecular representation of the scattering system the three-center molecular energy curves correlated to the AI states cannot cross the one related to X. The ADC process is therefore weak and less likely than double capture to ground or singly excited states (DC). For B^{3+} the autoionizing states are deeper than X and the strong repulsion from H_2^{2+} leads to efficient crossings between the related energy curves, although within a complex scenario due

TABLE I. Autoionizing states of He: the terms, leading electronic configurations, and energies (with respect to the ground state) of the doubly excited states used in our calculations. The two last columns show the values of the energies and the total widths from Lindroth [55].

Terms & leading configurations			Present work energy (eV)	Previous work Energy (eV)	Previous work Γ (eV)
^1S	$2s^2$	(71%)	57.67	57.63	1.2×10^{-1}
	$2p^2$	(22%)			
^1D	$2p^2$	(83%)	60.45	59.70	6.4×10^{-2}
^1P	$2s2p$	(79%)	60.86	59.94	3.7×10^{-2}
	$2p3s$	(17%)			
	$2p^2$	(42%)	62.49	61.88	5.9×10^{-3}
^1S	$2s3s$	(34%)			
	$2s^2$	(11%)			
	$2p3s$	(45%)	62.88	62.55	4.0×10^{-6}
^1P	$2s3p$	(38%)			
	$2p4s$	(12%)			
	$2s3s$	(36%)	63.00	62.75	3.7×10^{-2}
^1S	$2p3p$	(30%)			
	$2s4s$	(18%)			
	$2s^2$	(9%)			

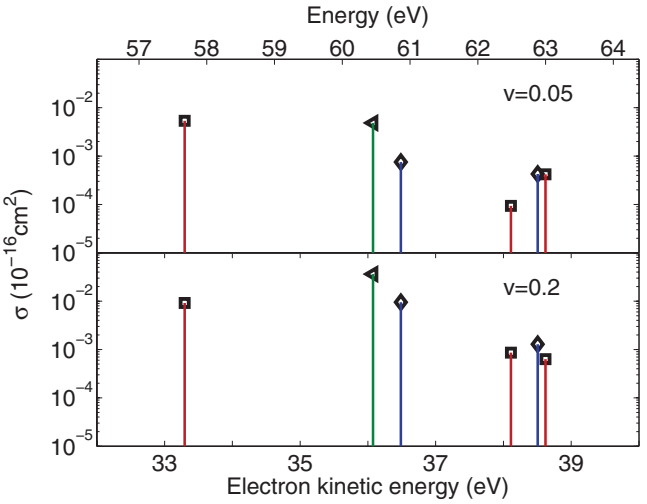

FIG. 3. (Color online) State-to-state ADC cross sections for the He^{2+} projectile: the cross sections are shown in logarithmic scale as functions of the state energy with respect to the He ground state (top axis) and as functions of ejected electron energy (bottom axis). For clarity the cross sections are marked with squares for ^1S states, diamonds for ^1P states, and triangles for ^1D states. The top (bottom) panel corresponds to impact velocity $v = 0.05$ ($v = 0.2$).

to the number of available channels. In the low energy domain considered, the ADC is indeed strong, about the same order of magnitude as single capture (SC), but slightly dominated by transfer-ionization, a process leaving B^{4+} in its L shell (not shown). Finally for Li^+ the situation is intermediate since the lowest and important doubly excited states lie close to X and can be populated by a direct mechanism for the largest energies considered while at low velocity the ADC is achieved through crossings with curves correlated to single capture and transfer-excitation (i.e., single capture accompanied with simultaneous target excitation [54]) channels. Note also that as for B^{3+} DC is again negligible with respect to the ADC.

Figures 3–5 show in detail the state-to-state ADC cross sections for the autoionizing states which have been identified and included in our calculations. Their respective (singlet) terms, leading electronic configurations, and energies, together with values of energy and lifetime found in the literature, are reported in Tables I to III. For the sake of clarity the cross sections are only shown for two typical velocities, the lowest value considered in this investigation ($v = 0.05$) and an intermediate one ($v = 0.2$).

A. He^{2+} projectile

Table I lists the He doubly excited states of importance in this paper. First it shows that the energies of the states created from our GTO basis set are in very good agreement—within 2% difference or less—with the reference values from Lindroth's investigation [55]. Figure 3 shows that the states which are mainly populated during the collision are related to the electronic configurations $2s^2$, $2p^2$, and $2s2p$. This is in qualitative (since no absolute measurements are available) agreement with the results and tendencies shown in [7] (for impact velocity $v \approx 0.6$) and [46] (for $v \approx 0.3$). At the highest velocity considered in this figure, the ADC is more selective and mainly populates the first ^1D state. At $v = 0.05$ the two

TABLE II. Autoionizing states of Li^+: the terms, leading electronic configurations, and energies (with respect to the ground state) of the doubly excited states used in our calculations. The two last columns show the values of the energies and the total widths from Diehl *et al.* [56].

	Terms & leading configurations		Present work energy (eV)	Previous works Energy (eV)	Previous works Γ (eV)
^1S	$2s^2$	(73%)	146.0	146.1	1.5×10^{-1}
	$2p^2$	(23%)			
^1D	$2p^2$	(93%)	150.4	149.9	1.6×10^{-2}
^1P	$2s2p$	(93%)	150.9	150.3	5.9×10^{-2}
^1S	$2p^2$	(65%)	154.3	153.8	6.6×10^{-3}
	$2s^2$	(22%)			
^1P	$2p3s$	(48%)	159.1	159.2	1.8×10^{-4}
	$2s3p$	(45%)			
^1S	$2s3s$	(61%)	159.4	159.7	5.9×10^{-2}
	$2p3p$	(25%)			
^1P	$2p3p$	(92%)	159.8	161.1	
^1D	$2p3p$	(66%)	161.0		
	$2p4p$	(30%)			
^1S	$2p4p$	(38%)	162.0	162.1	1.6×10^{-3}
	$2p3p$	(29%)			
	$2s4s$	(17%)			
	$2s3s$	(12%)			
^1S	$3s^2$	(67%)	174.5	174.3[a]	1.4×10^{-1} [a]
	$3p^2$	(27%)			
^1D	$3p^2$	(92%)	176.4	174.8[a]	2.3×10^{-1} [a]

[a]From Bachau *et al.* [57].

lowest ^1D and ^1P states evenly share the ADC probability. Note that same trends are observed with the smaller basis set presented in the Appendix. The relative weight of the bunch of states located at about 63 eV and corresponding to $2\ell n\ell'$ ($n \geqslant 2$) configurations is also decreasing with decreasing velocities. As already discussed the cross sections for the important states are rather weak so that this system cannot be considered as convenient to study interferences in the considered impact energy range.

B. Li^{3+} projectile

The doubly excited states of Li^+ included in our calculations are divided into two sets (cf. Table II). Nine levels lie between the first [$Li^{2+}(n = 1)$] and second [$Li^{2+}(n = 2)$] thresholds and are identified without ambiguity thanks to both the stabilization scheme used in the diagonalization and the excellent agreement (deviations smaller than 0.5%) with the data reported by Diehl and collaborators [56]. One can also see two levels which lie above the second ionization threshold and are found to be less accurately described by our GTO basis set: the differences with the data of Bachau and collaborators [57] reach 7% for the last identified ^1D state. This is not surprising since we do not include d orbitals in our basis sets while the weight of the $3s3d$ configuration is evaluated to be 35% in [57]. However these two high states are only very weakly populated in the scattering stage for the energy domain under consideration. Indeed one can see from Fig. 4 that the main contributions to the ADC stem from the lowest autoionizing states. This finding is similar to the results obtained for He and related to the low charge carried by the two projectiles and implying a moderate asymmetry between the collision partners in both cases. Another similarity between the two systems is related to the most likely channel: ADC cross sections are dominated by the ^1D $2p^2$ ones at $v = 0.2$, while the probability is evenly shared between this level and the ^1S $2s^2$ one at the lowest velocity, the weight of the other states decreasing significantly. Equivalent results are obtained with the smaller basis set reported in the Appendix.

TABLE III. Autoionizing states of B^{3+}: the terms, leading electronic configurations, and energies (with respect to the ground state) of the doubly excited states used in our calculations. The two last columns show the values of the energies and the total widths from Kramida *et al*. [58].

Terms & leading configurations			Present work	Previous works	
			energy (eV)	Energy (eV)	Γ (eV)
^1S	$2s^2$	(76%)	444.1	445.7	3.6×10^{-1}
	$2p^2$	(23%)			
^1D	$2p^2$	(98%)	451.9	452.6	3.0×10^{-1}
^1P	$2s2p$	(98%)	452.8	453.3	1.7×10^{-1}
^1S	$2p^2$	(73%)	459.0	459.8	1.6×10^{-2}
	$2s^2$	(23%)			
^1P	$2p3s$	(51%)	484.5	486.3	4.1×10^{-4}
	$2s3p$	(47%)			
^1S	$2s3s$	(71%)	485.0	487.1	1.6×10^{-1}
	$2p3p$	(25%)			
^1P	$2p3p$	(98%)	485.8		
^1D	$2p3p$	(98%)	488.4	489.4	8.8×10^{-2}
^1P	$2s3p$	(48%)	488.7	490.2	6.4×10^{-2}
	$2p3s$	(42%)			
^1S	$2p3p$	(61%)	491.0	492.3	5.4×10^{-3}
	$2s3s$	(21%)			
^1S	$2s4s$	(82%)	498.3		
	$2s5s$	(7%)			
^1P	$2p4s$	(84%)	498.4	492.3	
	$2p5s$	(10%)			
^1S	$2s6s$	(76%)	506.3		
	$2s7s$	(6%)			
	$2s5s$	(5%)			
^1D	$3p^2$	(98%)	532.0	529.2[a]	2.1×10^{-1} [a]
^1P	$3s3p$	(96%)	533.0	530.0[a]	3.7×10^{-1} [a]
^1S	$3p^2$	(66%)	535.6	528.4[a]	1.5×10^{-1} [a]
	$3s^2$	(30%)			
^1P	$3p4s$	(92%)	544.7	535.3[a]	9.0×10^{-2} [a]
^1S	$3s5s$	(87%)	545.0	531.7[a]	5.0×10^{-1} [a]

[a]From Bachau *et al*. [57].

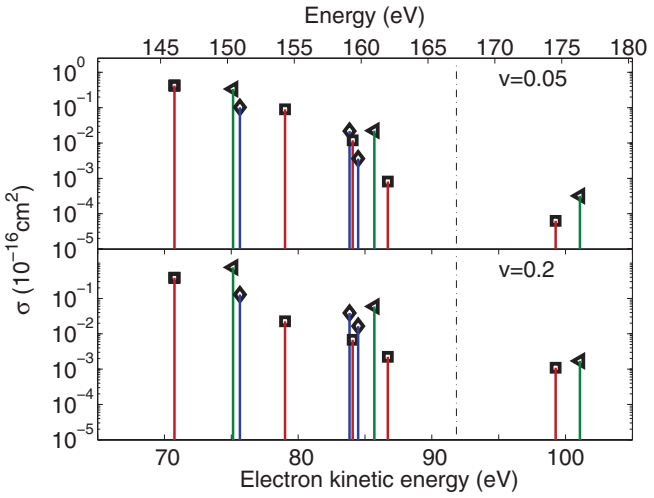

FIG. 4. (Color online) State-to-state ADC cross sections for the Li^{3+} projectile: same as Fig. 3. The electron energies are given with respect to the first ionization threshold, and the vertical dotted-dashed line marks the second ionization threshold.

C. B^{5+} projectile

Table III lists the different doubly excited states included in our calculations and compares them with two sets of data, from Kramida *et al.* [58] and Bachau *et al.* [57]. Our results are again in close agreement with the previous and specialized investigations, and though we do not include d orbitals to avoid extra immoderate computing time in the scattering calculations, the differences between the three sets of results are generally less than 1%, except for the highest level listed in the table for which the difference reaches about 2%. Note that the five highest states identified in our calculations are lying between $B^{4+}(n = 2)$ and $B^{4+}(n = 3)$ and were required to get a reasonable convergence of the results; indeed, as can be seen in Fig. 5, these states contributed to nearly 50% to the total ADC process. Note also that for this system the number

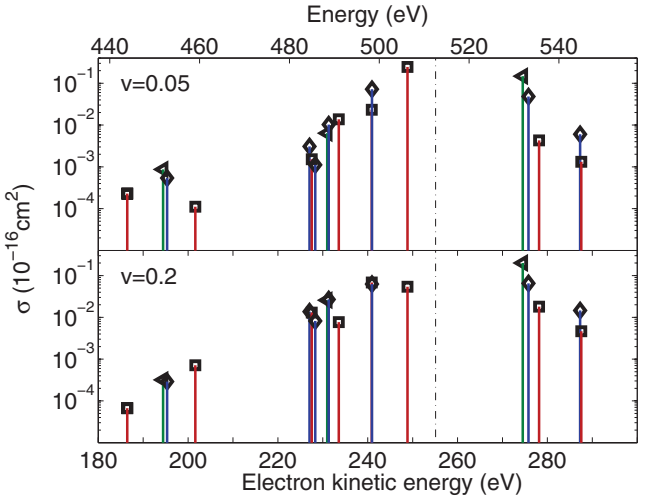

FIG. 5. (Color online) State-to-state ADC cross sections for the B^{5+} projectile: same as Fig. 3. The electron energies are given with respect to the first ionization threshold, and the vertical dotted-dashed line marks the second ionization threshold.

of nonequivalent electronic configurations possibly populated during the collision is larger that for the two first systems. Similar conclusions can be drawn from the results with the different basis set reported in the Appendix.

For this asymmetric charged system the general pattern describing the relative population of the different doubly excited states (covering an energy domain larger than 100 eV) is quite different compared to the two previous cases. Indeed as already mentioned this system experiences a complex series of crossings between the molecular curves related asymptotically to the initial and ADC channels. Among these crossings the important ones are those responsible for double capture to states lying just below and just above the second ionization threshold. Figure 5 shows this tendency: the AI states whose energies are above 512 eV (i.e., second threshold) contributing to about 35% to the ADC at the lowest energy, to 52% at $v = 0.2$, and up to 71% at $v = 0.6$ (not shown) where the ADC cross section reaches a maximum. For the two considered velocities one state dominates significantly the process with large cross sections: the $^1S\ 2sns$ $(n \geqslant 6)$ state (cross section of 0.25×10^{-16} cm^2) at $v = 0.05$ and the ^1D $3p^2$ state (0.20×10^{-16} cm^2) at $v = 0.2$. Double capture to this latter state still shows a significant cross section of about 0.15×10^{-16} cm^2 at the lowest velocity. Note finally that from the point of view of the magnitude of ADC cross sections and of the selectivity of the process (with one or two levels mainly populated), the two Li^{3+}-H_2 and B^{5+}-H_2 collision systems present large similarities and are good candidates for further investigations on ADC processes and postcollisional effects.

D. Discussion

As already mentioned the purpose of the present investigation is twofold: (i) a first step to describe the scattering processes producing doubly excited states entangled with their decay and (ii) a suggestion of collision systems in order to probe the formation of interference patterns at low impact energy when the ejection of electrons takes place within the scattering event [46]. These two points are of course closely related. We shall mainly focus our attention on state lifetime vs collision time, energy of the ejected electrons, and magnitude of the cross sections. Concerning the extension of the experimental investigation [7] to low impact energies, we shall not consider the parameters of *visibility* of interference fringes presented in Barrachina and Zitnik's original work [44] since their model is not appropriate for low energies.

The estimate of collision time can be done by considering the range of impact parameters in which the ADC processes occur. Though slightly depending on impact energy, the size of the collision zone where both partners charge cloud overlap can be roughly characterized by 10 a.u. which gives a collision time of about 5 fs (1 fs) for a collision velocity $v = 0.05$ a.u. (0.2 a.u.). The Auger linewidths of the two important states populated by the ADC (for each collision system) range from about 0.01 to 0.2 eV, corresponding to lifetimes from 60 to about 3 fs. These data show that only velocities in the range of the present lowest one, combined with the analysis of ADC process populating states of the largest linewidth, will enable to probe the new collision regime. In fact these criteria show also that our model which does not involve AI state decay during

the scattering event may not be valid for the lowest velocities considered. This conclusion supports the future development of models describing coherently the scattering and Auger decay stages.

On the other hand the de Broglie wavelength of the ejected electron does not seem to be a crucial criterion to study the back scattering process: indeed for He^{2+} (Li^{3+}, B^{5+}) the most populated AI states are located at about 35 eV from the first ionization threshold (75 and 250 eV, respectively), corresponding to a wavelength of 4 a.u. (2.7 and 1.4 a.u., respectively) to be compared with the internuclear H_2 distance, i.e., R_{eq}= 1.4 a.u. assuming the two protons only slightly falling apart in between capture and Auger decay. This is a rather good approximation for the systems under consideration since (i) for low impact energy the ejection takes place when the target and the projectile are still close and (ii) the velocity of the protons during the target explosion is one to two orders of magnitude smaller than the ones of the Auger electrons under consideration ($v_{e\mathrm{Auger}} > 2$ a.u.). Note however that for the B^{5+} projectile the important $^1D\ 3p^2$ states should mainly decay onto the second ionization threshold; cf. the partial linewidths listed in [57], giving rise to slower (20 eV) electrons, increasing the possibility to probe their scattering onto escaping protons.

Finally to go back to the two objectives of the present study, one can conclude that

(i) from the experimental point of view, Li^{3+} and B^{5+} projectiles seem to be good candidates to probe single electron interference phenomena at low impact energies. They present high cross sections for double capture into the respective $^1S\ 2s^2$ and $^1D\ 3p^2$ states which present optimal characteristics to probe complex secondary processes within the scattering stage. The He^{2+} projectile is clearly not a good candidate because of the strong decrease of the cross sections with decreasing impact energies;

(ii) for the further development of theory to describe these complex events, the three systems are of course relevant (the He $^1S\ 2s^2$ state is also a good candidate to probe the two correlated events) since the study of processes with small cross sections is not as critical as in experimental studies. In fact from a practical point of view (size of the GTO basis, number of states to involve in the coupled-channel scheme, and therefore CPU and memory considerations), it is rather the He^{2+} projectile which should be favored in future theoretical investigations.

IV. CONCLUSION

In the present paper we report the impact energy dependence of the cross sections of double electron capture into doubly excited states induced in collisions between moderately charged ions and dihydrogen molecules. A state-to-state analysis of the total cross sections is also performed and discussed in relation with the main features of the important states populated, i.e., the lifetime and ejected electron energy. Convergence of the results with respect to the basis set sizes was checked and discussed. The present results stem from a complex treatment modeling nonperturbatively the collision process. We have shown the limit of our model when considering the lowest part of the energy domain considered in the present work. These data represent benchmarks for future theoretical investigations including the behavior of the doubly excited states in the description of the scattering process. Finally different suggestions of optimal systems to guide future experimental studies of interference effects observable in an atomic-size two-center interferometer [46] are presented. These will also be benchmarks for theoretical development in order to describe the dynamics of complex highly correlated many-body quantum systems.

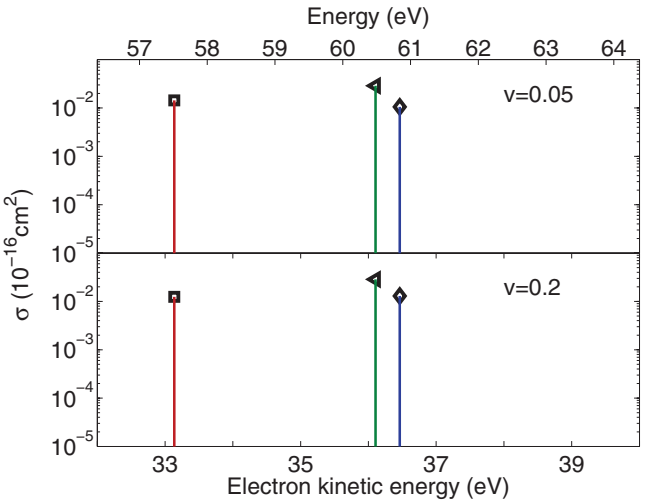

FIG. 6. (Color online) State-to-state ADC cross sections for the He^{2+} projectile: same as Fig. 3 but using a smaller GTO expansion; cf. Appendix.

ACKNOWLEDGMENTS

This work is supported by the Bergen Research Foundation (Norway). The research leading to these results has received funding from the EU Seventh Framework Programme under Grant No. PIRSES-GA-2010-269243.

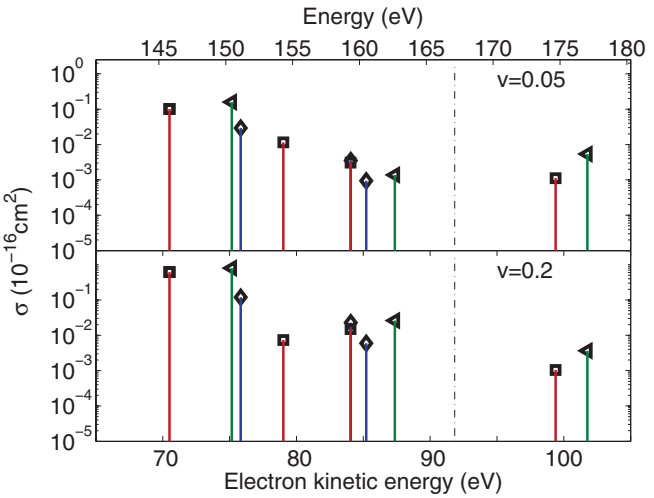

FIG. 7. (Color online) State-to-state ADC cross sections for the Li^{3+} projectile: same as Fig. 4 but using a smaller GTO expansion; cf. Appendix.

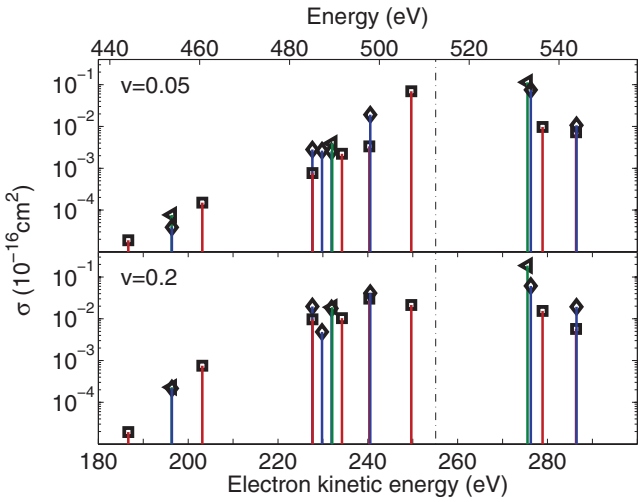

FIG. 8. (Color online) State-to-state ADC cross sections for the B^{5+} projectile: same as Fig. 5 but using a smaller GTO expansion; cf. Appendix.

APPENDIX

We present in the following one of the basis sets (named SBS hereafter) used to test the convergence of the results; they are built from smaller GTO expansions so that the number of states included in the calculations are less numerous, and the quality of the states is poorer in some cases, especially for the doubly excited ones we have focused on. In detail they are constructed from 10 $\ell = 0$ and 3×4 $\ell = 1$ GTOs (253 products and 53 states) for He^+ and He, from 12 $\ell = 0$ and 3×6 $\ell = 1$ GTOs (for 465 GTO products and 98 states) for Li^{2+} and Li^+, and from 12 $\ell = 0$ and 3×6 $\ell = 1$ GTOs (for 465 products and 278 states) for B^{4+} and B^{3+}.

For He doubly excited states, the three lowest ones are described nearly equivalently (with differences in energy lower than 0.1%) by both basis sets while the three higher ones were not identified by the stabilization scheme in SBS. For Li^+ and B^{3+} the convergence upon the energy of the doubly excited states is similar with a maximum difference of 1%, i.e., a shift of a maximum of 2 eV which can be seen when comparing Fig. 4 vs Fig. 7 (and Fig. 5 vs Fig. 8). In both cases some of the autoionizing states included in the large scale calculations were not identified in SBS and were considered as pseudostates in the analysis.

When comparing Figs. 6–8 with Figs. 3–5, respectively, significant differences in cross sections can be seen, especially for the low cross sections, i.e., below 10^{-18} cm^2. However the important ADC channels are found to be the same with both basis sets so that the conclusions drawn from the largest basis set for each system can be considered as reliable and are not basis dependent. We tend to think that it is not the differences between the autoionizing states from both types of basis sets which explain the differences found in cross sections but the number of states included in the scattering stage. Indeed for He, the ADC is weak compared to DC and SC so that a 10% change in the important channel cross sections changes dramatically the ADC ones. For Li and B we have shown that avoided crossings are important to explain the important ADC channels observed in the low energy range considered: it is known that a slight modification of the geometry of the crossing regions due to increase or decrease of the number of GTOs may change significantly the transition probabilities. We should conclude that the largest basis sets are optimal to describe the important ADC channels under consideration, as well as DC and SC. Further calculations with larger basis sets will lead to similar conclusions to the ones drawn here but will improve the convergence of the cross sections. They are out of reach in the present time.

[1] M. Drescher *et al.*, Nature (London) **419**, 803 (2002).
[2] J. F. Pérez-Torres, J. L. Sanz-Vicario, H. Bachau, and F. Martín, J. Phys. B **43**, 015204 (2010).
[3] M. Førre *et al.*, J. Phys. B **35**, 401 (2002).
[4] O. Sise, M. Dogan, I. Okur, and A. Crowe, Phys. Rev. A **84**, 022705 (2011).
[5] L. Ishikawa *et al.*, J. Phys. B **44**, 065203 (2011).
[6] H. A. Sakaue *et al.*, J. Phys. B **24**, 3787 (1991).
[7] J.-Y. Chesnel, A. Hajaji, R. O. Barrachina, and F. Frémont, Phys. Rev. Lett. **98**, 100403 (2007).
[8] D. S. Fisher, C. W. Fehrenbach, S. R. Lundeen, E. A. Hessels, and B. D. DePaola, Phys. Rev. Lett. **81**, 1817 (1998).
[9] B. Bederson, Comm. At. Mol. Phys. **1**, 65 (1969).
[10] J. P. Connerade, *Highly Excited Atoms* (Cambridge University Press, Cambridge, 2005).
[11] G. Tanner, K. Richter, and J.-M. Rost, Rev. Mod. Phys. **72**, 497 (2000).
[12] D. Belkić, I. Mančev, and J. Hanssen, Rev. Mod. Phys. **80**, 249 (2008).
[13] M. Mack *et al.*, Phys. Rev. A **39**, 3846 (1989).
[14] M. Barat and P. Roncin, J. Phys. B **25**, 2205 (1992).
[15] S. Martin, J. Bernard, L. Chen, A. Denis, and J. Désesquelles, Phys. Rev. A **52**, 1218 (1995).
[16] P. Moretto-Capelle, M. Benhenni, D. Bordenave-Montesquieu, and A. Bordenave-Montesquieu, J. Phys. B **29**, 2007 (1996).
[17] J. Y. Chesnel *et al.*, Nucl. Instrum. Meth. B **154**, 142 (1999).
[18] P. Moretto-Capelle, D. Bordenave-Montesquieu, and A. Bordenave-Montesquieu, J. Phys. B **33**, L735 (2000).
[19] T. Kusakabe, Y. Miyamoto, M. Kimura, and H. Tawara, Phys. Rev. A **73**, 022706 (2006).
[20] S. Figueira da Silva, H. P. Winter, and F. Aumayr, Phys. Rev. A **75**, 042706 (2007).
[21] S. Martínez, G. Bernardi, P. Focke, S. Suárez, and D. Fregenal, J. Phys. B **41**, 145204 (2008).
[22] Y.-L. Xue *et al.*, Chin. Phys. Lett. **27**, 073402 (2010).
[23] L. F. Errea, L. Fernández, A. Macías, L. Méndez, I. Rabadán, and A. Riera, Phys. Rev. A **69**, 012705 (2004).
[24] S. Martínez, G. Bernardi, P. Focke, A. D. González, and S. Suárez, J. Phys. B **35**, 2261 (2002).

[25] W. Fritsch and C. D. Lin, Phys. Rep. **202**, 1 (1991).
[26] B. H. Bransden and M. R. C. McDowell, *Charge Exchange and the Theory of Ion-Atom Collisions* (Oxford University Press, Oxford, 1992).
[27] W. Fritsch and C. D. Lin, J. Phys. B **19**, 2683 (1986).
[28] K. Moribayashi, K.-I. Hino, M. Matsuzawa, and M. Kimura, Phys. Rev. A **44**, 7234 (1991).
[29] S. E. Nielsen, J. P. Hansen, and A. Dubois, J. Phys. B **28**, 5295 (1995).
[30] F. Martin and A. Salin, J. Phys. B **28**, 639 (1995).
[31] C. Harel and H. Jouin, Europhys. Lett. **11**, 121 (1990).
[32] M. V. Khoma, V. Y. Lazur, and R. K. Janev, Phys. Rev. A **80**, 032706 (2009).
[33] L. F. Errea, J. D. Gorfinkiel, A. Macías, L. Méndez, and A. Riera, J. Phys. B **30**, 3855 (1997).
[34] M. Nagao, K. N. Hida, M. Kimura, S. N. Rai, H. P. Liebermann, R. J. Buenker, H. Suno, and P. C. Stancil, Phys. Rev. A **78**, 012708 (2008).
[35] F. Martín, O. Mó, A. Riera, and M. Yáñez, Phys. Rev. A **38**, 1094 (1988).
[36] Z. Chen and C. D. Lin, Phys. Rev. A **48**, 1298 (1993).
[37] I. Sánchez and H. Bachau, J. Phys. B **28**, 795 (1995).
[38] C.-N. Liu, M.-K. Chen, and C. D. Lin, Phys. Rev. A **64**, 010501 (2001).
[39] D. R. Dewitt *et al.*, J. Phys. B **28**, L147 (1995).
[40] E. Lindroth *et al.*, J. Phys.: Conf. Ser. **194**, 012001 (2009).
[41] M. Boudjema *et al.*, J. Phys. B **22**, L121 (1989).
[42] H. Bachau, P. Roncin, and C. Harel, J. Phys. B **25**, L109 (1992).
[43] M. Ourdane, H. Bachau, R. Gayet, and J. Hanssen, J. Phys. B **32**, 2041 (1999).
[44] R. O. Barrachina and M. Zitnik, J. Phys. B **37**, 3847 (2004).
[45] A. Salin, Nucl. Instrum. Meth. B **86**, 1 (1994).
[46] F. Frémont *et al.*, Nucl. Instrum. Meth. B **267**, 206 (2009).
[47] R. O. Barrachina, F. Frémont, K. Fossez, D. Gruyer, V. Helaine, A. Lepailleur, A. Leredde, S. Maclot, G. Scamps, and J Y. Chesnel, Phys. Rev. A **81**, 060702(R) (2010).
[48] N. Sisourat, I. Pilskog, and A. Dubois, Phys. Rev. A **84**, 052722 (2011).
[49] For the Li and B ions, the actual sets of GTOs and list of states used in the calculations can be sent under request. For H_2 and He ions, we used the same basis sets as the ones described in detail in [48].
[50] A. U. Hazi and H. S. Taylor, Phys. Rev. A **1**, 1109 (1970).
[51] C. H. Maiert, L. S. Cederbaum, and W. Domcke, J. Phys. B **13**, L119 (1980).
[52] M. Garcia-Sucre and R. Lefebvre, Chem. Phys. Lett. **130**, 240 (1986).
[53] P.-O. Löwdin, J. Mol. Spectosc. **3**, 46 (1959).
[54] For the Li^{3+} projectile the main transfer-excitation channels correspond to transfer to the L shell of Li^{2+} with excitation mainly to the two first (dissociative) excited states of H_2^+.
[55] E. Lindroth, Phys. Rev. A **49**, 4473 (1994).
[56] S. Diehl *et al.*, J. Phys. B **32**, 4193 (1999).
[57] H. Bachau, F. Martín, A. Riera and M. Yáñez, Atom. Data Nucl. Data **48**, 167 (1991).
[58] A. E. Kramida *et al.*, Phys. Scr. **78**, 025302 (2008).